Available online at www.sciencedirect.com
ScienceDirect
Composites Science and Technology 67 (2007) 2399–2407
COMPOSITES SCIENCE AND TECHNOLOGY
www.elsevier.com/locate/compscitech

Mechanical characterization of graphite/epoxy nanocomposites by multi-scale analysis

J. Cho, J.J. Luo, I.M. Daniel *

Center for Intelligent Processing of Composites, McCormick School of Engineering and Applied Science, Northwestern University, Evanston, IL 60208, USA

Received 12 September 2006; received in revised form 2 January 2007; accepted 11 January 2007
Available online 30 January 2007

Abstract

Mechanical properties of nanocomposites consisting of epoxy matrix reinforced with randomly oriented graphite platelets were studied by the Mori–Tanaka approach in conjunction with molecular mechanics. Elastic constants of graphite nanoplatelets, which are the inclusion phase in the micromechanical model, were calculated based on their molecular force field. The calculated elastic constants compared well with both experimental data and other published theoretical predictions. The results of the Mori–Tanaka micromechanical analysis, using the graphite platelet moduli calculated by molecular mechanics, were found to be insensitive to the variation of out-of-plane modulus E_3 and Poisson's ratio ν_{13}. However, the nanocomposite modulus is sensitive to the in-plane modulus E_1 and out-of-plane shear modulus G_{13} of the graphite platelets and less sensitive to the in-plane Poisson's ratio ν_{12} for its small range of variation under consideration. The calculations confirm that the modulus of the nanocomposites studied here is strongly dependent on the aspect ratio of the reinforcing particles, but not on their size. The predicted moduli compare favorably with experimental results of several nanocomposites with graphite particles of various aspect ratios and sizes.

Keywords: A. Nanostructures; A. Polymer–matrix composites; B. Mechanical properties; B. Modeling; C. Elastic properties

1. Introduction

Graphite platelets are often used in polymeric matrices to enhance mechanical properties and impart physical functionalities such as electrical and thermal conductivities [1–4]. However, it is not easy to intuitively predict the mechanical properties of the resulting nanocomposites due to the anisotropic properties and morphology of the particles. Thus, it is desirable to carry out analytical or numerical analyses to understand how the particles affect the mechanical behavior of the composite.

Multi-scale analyses have been conducted for nanoparticle reinforced polymeric composites by incorporating molecular mechanical models into continuum models in recent years [5–8]. In general, the mechanical properties of nanostructured particles, expressed with atomic structures for the calculation, were evaluated by molecular mechanical analysis and subsequently, the nanoparticles were treated as equivalent solid particles, embedded in the polymeric matrix. The mechanical properties of the nanocomposite [5,6] and the load-transfer between the particles and matrix [7,8] were investigated with analytical and/or numerical micromechanical models.

In this study, following a similar analysis scheme, the elastic constants of graphite nanoplatelets were calculated based on molecular mechanics and subsequently, used in a micromechanical model based on the Mori–Tanaka method to calculate elastic constants of the nanocomposite [9]. We adopted the continuum approach because the dimensions of the platelet surface and edge are in the micrometer range, which allows for a large number of binding sites between the platelet and epoxy and justifies the continuum assumption. With the established model, the aspect ratio effect of the graphite particles on the elastic moduli of their composites was investigated. In addition,

* Corresponding author. Tel.: +1 847 491 5649; fax: +1 847 491 5227.
E-mail address: imdaniel@northwestern.edu (I.M. Daniel).

0266-3538/$ - see front matter © 2007 Elsevier Ltd. All rights reserved.
doi:10.1016/j.compscitech.2007.01.006

the effect of out-of-plane elastic constants of the nanoparticles was investigated, since, unlike in-plane elastic constants, there is a wide scatter in reported out-of-plane constants [10–18].

The experimental verification of the model was carried out with nanocomposites processed with two different types of particles, "as-received" and "intercalated and exfoliated". They provided different aspect ratios for evaluation of their effect.

2. Elastic properties of graphite

2.1. Structure of graphite

Graphite has a layered structure, as shown in Fig. 1. In a layer, carbon atoms are arranged in a hexagonal pattern with the shortest distance between atoms being 1.42 Å. The unit cell of the layer is hexagonal and comprises two atoms. In hexagonal graphite, the layers are stacked along the thickness direction (c-axis) in the so-called AB sequence. Each AB-layer is formed from an A layer by displacing it along the c-axis by half the crystallographic c-axis spacing of 3.35 Å and translating it in parallel by a distance equal to one side of the hexagon [19]. Here, the carbon layers are often called graphene layers or graphene sheets.

Carbon atoms in a graphene sheet are covalently bonded by sp^2 hybridized electrons, and their bond angle is 120° as illustrated in Fig. 1. This C–C bond in a graphene sheet is stronger than a single covalent C–C bond [20]. Adjacent graphene sheets are held together by weak van der Waals bonds, thus, the graphite displays softness along the c-axis and the graphene sheets can easily slide with respect to each other.

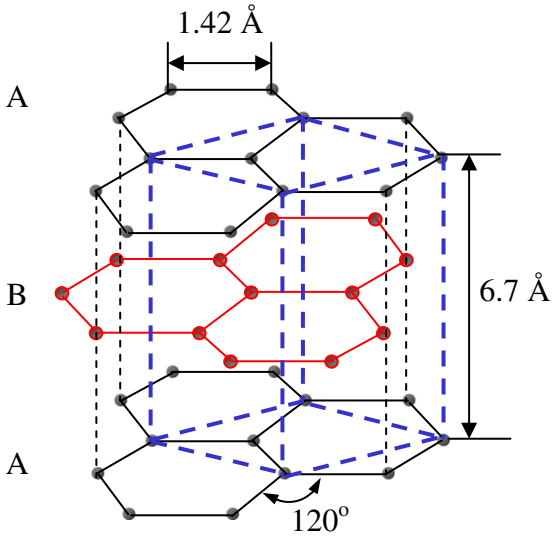

Fig. 1. Graphite structure.

2.2. Molecular mechanical analysis

2.2.1. Interatomic potential functions

Molecular mechanics is an approach for investigating the mechanical behavior of a material in nanoscale. In molecular mechanics, the interaction between atoms is modeled in terms of energy associated only with their nuclear positions. The total potential energy of graphite can be expressed as a sum of several energy terms;

$$U_t = U_{bond} + U_{angle} + U_{torsion} + U_{inversion} + U_{non\text{-}bonded}, \quad (1)$$

where U_{bond}, U_{angle}, $U_{torsion}$, and $U_{inversion}$ are potential energies associated with bond-stretching between two bonded atoms, angle-bending by three neighboring atoms, angle variation between two planes formed by four neighboring atoms, and also angle variation of two planes formed by four atoms where one atom is bonded to the other three, respectively; $U_{non\text{-}bonded}$ may include energies by non-bonded atoms typically due to the van der Waals and electrostatic interactions.

For graphite under in-plane loading (loading in the 1- or 2-direction in Fig. 2), the bond-stretching and angle-bending energy terms (U_{bond} and U_{angle}) are assumed to contribute significantly to the total potential energy. Several potential functions are available to describe the energy terms U_{bond} and U_{angle}, such as the harmonic [21], Tersoff–Brenner [22], EAM (Embedded Atom Method) [23], and modified Morse [24] potential functions. Generally, the Tersoff–Brenner potential function is more accurate and versatile for describing the C–C bond in a graphene sheet. However, it is cumbersome to implement the necessary numerical calculations.

The analysis was somewhat simplified by Belytschko et al. [24] who adopted the Morse potential function and added an angle-bending term to stabilize the structure of the carbon nanotube for the study of fracture behavior of single-walled carbon nanotubes. They chose its constants to emulate Brenner's potential function for strains below 10%. The constants of the angle-bending energy in the modified Morse potential function were further

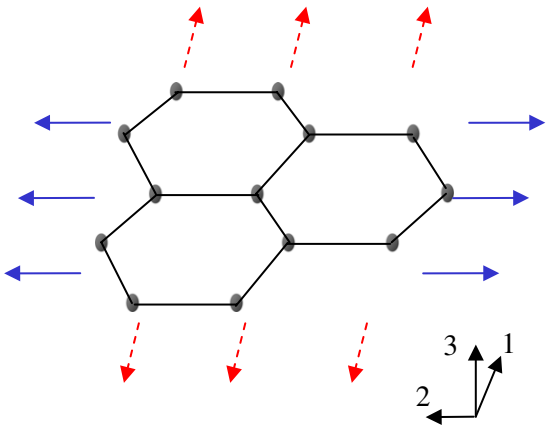

Fig. 2. Graphite under in-plane loading.

modified by Xiao et al. [25] based on Chang and Gao's model [21] to make the potential function more suitable for studying the elastic behavior of carbon nanotubes.

In this study, the modified Morse potential function and its constants by Xiao et al. [25] were adopted to describe the in-plane elastic behavior of graphite and are given as follows:

$$U_{\text{in-plane}} = D\left\{\left[1-\mathrm{e}^{-\beta(\Delta r)}\right]^2 - 1\right\} + \frac{1}{2}k_{\theta 1}(\Delta\theta)^2\left[1 + k_{\theta 2}(\Delta\theta)^4\right], \tag{2}$$

where $D = 6.031$ nN Å, $\beta = 2.625$ Å^{-1}, $k_{\theta 1} = 14.2$ nN Å/rad^2, and $k_{\theta 2} = 0.754$ rad^{-4}; Δr is the variation of bonding length between bonded carbon atoms; $\Delta\theta$ is the variation of the angle formed by three neighboring atoms.

For out-of-plane deformation, such as uniaxial deformation along the 3-axis or shear deformation between graphene sheets on the 1–2 plane, as seen in Fig. 3, non-bonded atomic interaction accounts for the main contribution to the total potential energy. The carbon atoms in adjacent graphene sheets physically interact with each other by the van der Waals force field. This non-bonded atomic interaction can be expressed using a Lennard–Jones potential function,

$$U_{\text{vdW}} = 4u\left[\left(\frac{r_0}{r_{ij}}\right)^{12} - \left(\frac{r_0}{r_{ij}}\right)^{6}\right], \tag{3}$$

where u is the well-depth determining the strength of interaction; r_0 indicates the equilibrium distance of two atoms that makes the potential equal to zero; r_{ij} is the distance between interacting atoms i and j.

In this study, we used the potential constants $u = 3.825 \times 10^{(-3)}$ nN Å (2.387 meV) and $r_0 = 3.42$ Å, which were determined by Girifalco and Lad [26] through various lattice summations for graphite with infinite number of graphene sheets.

2.2.2. Molecular structural analysis: in-plane elastic constants

The in-plane elastic behavior of graphite can be represented by that of a graphene sheet due to the small influence from adjacent graphene sheets by the weak van der Waals force field. Chang and Gao [21] developed a simple and effective analytical molecular mechanics model of a graphene sheet to calculate Young's modulus and Poisson's ratio of single-walled carbon nanotubes as a function of the nanotube diameter. In their model, the force-stretching relation of carbon atoms was modeled with elastic sticks of infinite bending stiffness, and the twisting moment-angle variation of carbon bonds was modeled with spiral springs. They called it "stick-spiral" model. Incorporating this model in the modified Morse potential function, Xiao et al. [25] obtained the stress–strain relation of single-walled carbon nanotubes as a function of the nanotube diameter.

It needs to be mentioned that the stick-spiral model describes the force–deformation response of a graphene sheet, which is a discrete system. In order to express its force–deformation relation in terms of an engineering stress–strain relation, this discrete system needs to be replaced with an effective continuum medium that can represent the volume occupied by the discrete system. Plates composed of graphene sheets have been used to derive engineering stress–strain relations from the force–deformation relations of the graphene sheets.

In this paper, we followed the work by Xiao et al. [25] and simplified the model for graphite platelets under infinitesimal deformation.

The force–deformation response of a graphene sheet can be analyzed with the representative elements shown in Fig. 4. Under loading, forces and moments acting on the atoms are obtained from their relative displacements as

$$F(\Delta r) = 2\beta D(1-\mathrm{e}^{-\beta\Delta r})\mathrm{e}^{-\beta\Delta r}, \tag{4}$$

$$M(\Delta\theta) = k_{\theta 1}\Delta\theta\left[1 + 3k_{\theta 2}(\Delta\theta)^4\right], \tag{5}$$

by differentiating the potential energy given in Eq. (2). For infinitesimal deformation, noting that $\Delta\theta$ is much smaller than unity, the higher order term of $\Delta\theta$ in Eq. (5) can be neglected. Rewriting Eq. (5), we have for the moment

$$M(\Delta\theta) = k_{\theta 1}\Delta\theta. \tag{6}$$

The deformed shape of the graphene sheet is determined by the equilibrium conditions of this force and moment together with the deformation constraints.

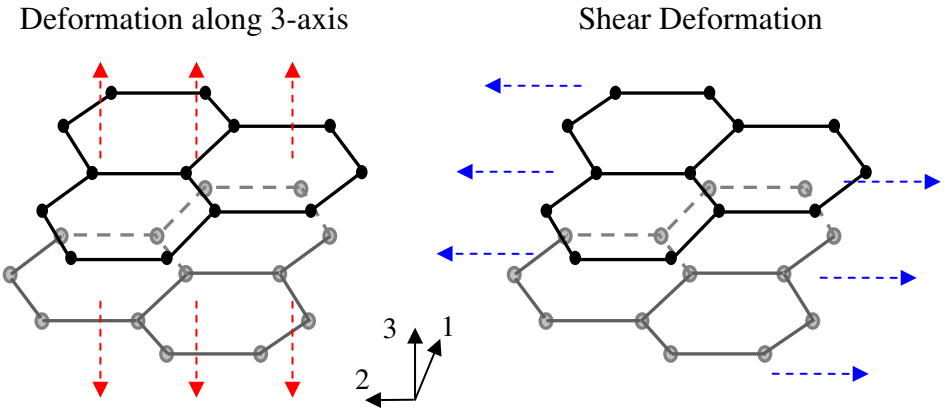

Fig. 3. Graphite under out-of-plane loading.

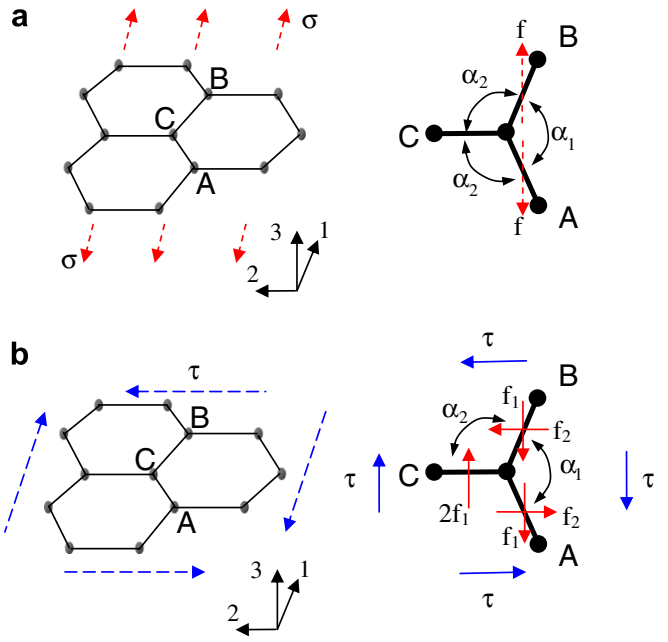

Fig. 4. Representative elements of a graphene sheet: (a) loading in the 1-direction and (b) shear loading in the 1–2 plane.

For uniaxial tension in the 1-direction in Fig. 4a, the equilibrium condition is

$$\left(\frac{b}{2}\right)F(\Delta b) = \tan\left(\frac{\alpha_1}{2}\right)[M(\Delta\alpha_1) - M(\Delta\alpha_2)], \tag{7}$$

where b is the bond length (1.42 Å); Δb is the variation of the bond length; α_1 is the angle of the carbon bonds (120 °C); $\Delta\alpha_1$ and $\Delta\alpha_2$ are the angle variations of the bonds which are related as

$$\Delta\alpha_1 = -2\Delta\alpha_2. \tag{8}$$

From Eqs. (4), (6), (7) and (8), the relationship between the bond-length and the bond-angle variation (Δb and $\Delta\alpha_1$, respectively) is written as

$$\Delta\alpha_1 = \left(\frac{2b}{3}\right)\frac{[\beta D(1-\mathrm{e}^{-\beta\Delta b})\mathrm{e}^{-\beta\Delta b}]}{k_{\theta 1}}\cot\left(\frac{\alpha_1}{2}\right). \tag{9}$$

With $\Delta\alpha_1$ obtained from the given Δb, the in-plane strains and axial stress can be calculated as

$$\varepsilon_{11} = \frac{\sin\left(\frac{\alpha_1}{2}\right)\Delta b + \frac{b}{2}\cos\left(\frac{\alpha_1}{2}\right)\Delta\alpha_1}{b\sin\left(\frac{\alpha_1}{2}\right)},$$
$$\varepsilon_{22} = \frac{\cos\left(\frac{\alpha_1}{2}\right)\Delta b - \frac{b}{2}\sin\left(\frac{\alpha_1}{2}\right)\Delta\alpha_1}{a + b\cos\left(\frac{\alpha_1}{2}\right)}, \tag{10}$$
$$\sigma_{11} = \frac{F(\Delta b)}{tb\sin\left(\frac{\alpha_1}{2}\right)\left(1+\cos\left(\frac{\alpha_1}{2}\right)\right)}, \tag{11}$$

where a is the bond length (1.42 Å) and t is the thickness (3.35 Å).

For the shear loading shown in Fig. 4b, the equilibrium conditions and deformation constraint are

$$\left(\frac{b}{2}\right)F(\Delta a) = \frac{1+\cos\left(\frac{\alpha_1}{2}\right)}{\sin\left(\frac{\alpha_1}{2}\right)}M(\Delta\alpha_2), \tag{12}$$

$$F(\Delta a) = -F(-\Delta b), \tag{13}$$

$$\Delta\alpha_2 = \frac{b[\beta D(1-\mathrm{e}^{-\beta\Delta a})\mathrm{e}^{-\beta\Delta a}]}{k_{\theta 1}}\left[\frac{\sin\left(\frac{\alpha_1}{2}\right)}{1+\cos\left(\frac{\alpha_1}{2}\right)}\right]. \tag{14}$$

The shear stress and strain are calculated from Eqs. (12)–(14) as

$$\gamma_{12} = \frac{c\Delta\alpha_1 + \sin\left(\frac{\alpha_1}{2}\right)\Delta b}{a\left(1+\cos\left(\frac{\alpha_1}{2}\right)\right)} + \frac{(\Delta a + \Delta b)\cos\left(\frac{\alpha_1}{2}\right)}{2b\sin\left(\frac{\alpha_1}{2}\right)}, \tag{15}$$

$$\tau_{12} = \frac{F(\Delta a)}{ta\left(1+\cos\left(\frac{\alpha_1}{2}\right)\right)}, \tag{16}$$

where c is the bond length (1.42 Å).

To determine Young's modulus, $E_1 = \sigma_{11}/\varepsilon_{11}$, and Poisson's ratio $\nu_{12} = -\varepsilon_{22}/\varepsilon_{11}$, a strain of $\varepsilon_{11} = 0.1\%$ was used. The in-plane Young's modulus and Poisson's ratio were calculated to be 1.153 TPa and 0.195, respectively. Similarly, by taking the ratio of the shear stress to shear strain for a shear strain of 0.1%, $G_{12} = \tau_{12}/\gamma_{12}$ the in-plane shear modulus was determined to be 0.482 TPa. The engineering constants, listed in Table 1, are in good agreement with both experimental and other published theoretical predictions [10,16,21,25]. In addition, it can be seen that the relationship between the in-plane shear modulus, Young's modulus and Poisson's ratio for an isotropic material, $G_{12} = E_1/2(1+\nu_{12})$, is satisfied. This is a consequence of the hexagonal array of atoms in a graphene sheet.

2.2.3. Molecular structural analysis: out-of-plane elastic constants

Referring to the coordinate notation in Fig. 3 and assuming transverse isotropy of the graphite plates, the out-of-plane elastic constants to be determined are E_3, G_{13} (=G_{23}), and ν_{13} (=ν_{23}).

The moduli E_3 and G_{13} can be expressed as

$$E_3 = \frac{C_{33}C_{11} + C_{12}C_{33} - 2C_{13}^2}{C_{11}+C_{12}} \quad \text{and} \quad G_{13} = C_{44}, \tag{17}$$

where C_{ij} are stiffness components in the generalized Hooke's law. Knowing the in-plane elastic constants E_1 and ν_{12}, we can rewrite the expression for the modulus E_3 as

$$E_3 = \frac{(1-\nu_{12})E_1C_{33}}{(1-\nu_{12})E_1 + 2\nu_{13}^2C_{33}}. \tag{18}$$

Table 1
In-plane elastic constants of graphite

Elastic constants	Present	Ref. [10]	Ref. [16]	Ref. [21]	Ref. [25]
E ($E_1 = E_2$), TPa	1.153	1.02	0.90	1.06	1.13
ν_{12}	0.195	0.16	0.039	0.16	0.20
G_{12}, GPa	0.482	0.44	0.43	n/a	0.47

The stiffness components C_{33} and C_{44} and Poisson's ratio ν_{13} need to be calculated from Eqs. (17) and (18) to determine E_3 and G_{13}.

In the calculations of C_{33} and C_{44}, we followed Kelly and Duff [14] who applied the Lennard–Jones potential [26,27] to determine the interaction between carbon atoms in adjacent graphene sheets and calculated C_{33} and C_{44} from the second derivatives of the strain energy density with respect to ε_{33} and γ_{13}, respectively.

Considering two adjacent graphene sheets, the interaction of a carbon atom in one graphene sheet with all the atoms in the other sheet can be obtained from Eq. (3) as

$$U_{\mathrm{vdW}} = 4ur_0^6\left[r_0^6 S_{12} - S_6\right], \tag{19}$$

where

$$S_n = \sum_j r_j^{-n} = \sum_j (d^2 + l_j^2)^{-\frac{n}{2}}, \tag{20}$$

where d is the distance between two graphene sheets on the c-axis and l_j $(= \sqrt{x_j^2 + y_j^2})$ is the radial distance of the jth atom in the graphene sheet from the point directly above or below the considered atom in the neighbor graphene sheet.

It is seen in Fig. 1 that there are two types of equilibrium for an atom adjacent to a graphene sheet. One is when the atom is vertically over the center of a hexagon, the other is when the atom is above a vertex of a hexagon. In order to calculate the energy density, defined as the energy/unit volume of a crystal [27], the potential energies obtained from the atoms in two different equilibrium positions are averaged, and the energy density is given as

$$\Phi = \frac{4ur_0^6}{dA}\left[r_0^6 \overline{S}_{12} - \overline{S}_6\right], \tag{21}$$

where $\overline{S}_n$ is the average of the summation for the two equilibrium positions, and A is the area/atom in a graphene sheet ($A = 2.62$ Å^2).

From the second derivatives of Eq. (21) with respect to ε_{33} and γ_{13}, and by approximation in the Taylor series expansion of function Φ, C_{33} and C_{44} are obtained as

$$C_{33} = \frac{\partial^2 \Phi}{\partial \varepsilon_{33}^2} \cong d_0^2 \left(\frac{\partial^2 \Phi}{\partial d^2}\right)_{d=d_0}, \tag{22}$$

$$C_{44} = \frac{\partial^2 \Phi}{\partial \gamma_{13}^2} \cong d_0^2 \left(\frac{\partial^2 \Phi}{\partial x_j^2}\right)_{x_j = x_j^0}, \tag{23}$$

where

$$\frac{\partial^2 \overline{S}_n}{\partial d^2} = -n\overline{S}_{n+2} + n(n+2)d^2\overline{S}_{n+4}, \tag{24}$$

$$\frac{\partial^2 \overline{S}_n}{\partial x_j^2} = -n\overline{S}_{n+2} + n(n+2)\sum_j \frac{x_j^2}{(d_0^2 + x_j^2 + y_j^2)^{\frac{(n+4)}{2}}}, \tag{25}$$

and d_0 and x_j^0 are the distances in the undeformed state.

Poisson's ratio $\nu_{13} = -\varepsilon_{33}/\varepsilon_{11}$ must be evaluated from the deformation in the thickness direction corresponding to an applied strain ε_{11}. A straightforward calculation was performed by first applying a small deformation in the 1-direction using Eq. (10), as shown in Fig. 5. Subsequently, the average energy density was calculated by Eq. (21). Since the deformed state corresponds to a minimum energy state, the distance, d_z, of the considered graphene sheet minimizing the energy density under in-plane deformation was evaluated as

$$\frac{\partial \Phi}{\partial d} = \frac{4ur_0^6}{dA}\left[\left(r_0^6 \frac{\partial \overline{S}_{12}}{\partial d} - \frac{\partial \overline{S}_6}{\partial d}\right) - \frac{1}{d}\left(r_0^6 \overline{S}_{12} - \overline{S}_6\right)\right] = 0 \quad \text{at } d = d_z, \tag{26}$$

where

$$\frac{\partial \overline{S}_n}{\partial d} = -nd\overline{S}_{n+2}. \tag{27}$$

Then, this distance was used to obtain ε_{33}, followed by calculation of ν_{13}. Fig. 6 shows the strain development in the thickness direction as a function of the in-plane strain. Poisson's ratio ν_{13} is calculated from the slope of the curve.

Table 2 shows that the out-of-plane elastic constants E_3, G_{13} $(=G_{23})$, and ν_{23} $(=\nu_{23})$ were calculated to be 39.511 GPa, 0.268 GPa and 0.006, respectively. Comparing with the data in Refs. [10–18], the Young's modulus E_3 is in fairly good agreement with the literature data, and the shear modulus G_{13} and Poisson's ratio ν_{13} fall in the wide range of the literature data.

In Table 2, the shear modulus G_{13} varies from 0.13 GPa to 4.5 GPa. As discussed in [10], the shear modulus of perfect graphite is 4.5 GPa, but it is reduced due to the mobile dislocation in the basal plane of the graphite crystal. It is believed that the calculation of G_{13} by the Lennard–Jones potential underestimates the true value of G_{13} of graphite. As mentioned in [11], this is because the interlayer force constant of adjacent graphene sheets by the Lennard–Jones potential is substantially lower than that with interlayer lattice vibrations observed by neutron spectrometry.

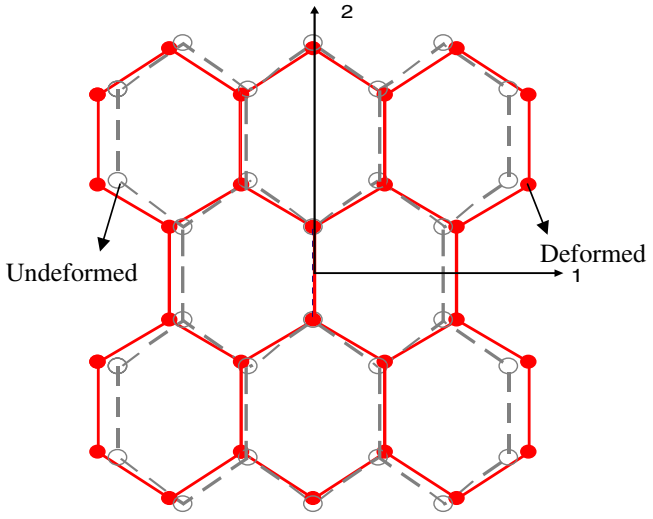

Fig. 5. Deformation of a graphene sheet in the 1-direction, ε_{11}=0.1.

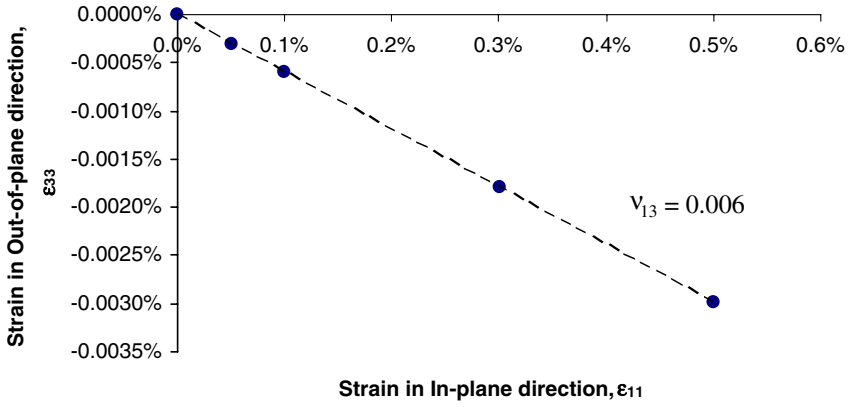

Fig. 6. Development of ε_{33} strain in the 3-direction as a function of in-plane strain ε_{11}.

Table 2
Out-of-plane elastic constants of graphite

Elastic constants	Present	Ref. [10]	Ref. [11]	Ref. [12]	Ref. [13]	Ref. [14]	Ref. [15]	Ref. [16]	Ref. [17]	Ref. [18]
E_3, GPa	39.511	36.4	39.0	55.8	n/a	38.6	20.3–35.6	30.2	n/a	17.1
v_{13} (=v_{23})	0.006	0.337	n/a	−0.171[a]	n/a	n/a	n/a	2.248	0.822	4.958[b]
v_{31} (=v_{32})	0.0002	0.012	n/a	0.0084[a]	n/a	n/a	n/a	0.075	0.019	0.074
G_{13} (=G_{23}), GPa	0.268	0.28	4.2	n/a	0.13	0.23	0.7–4.5	2.3	n/a	n/a

[a] E_1 and v_{12} from present study were used to calculate the Poisson's ratios according to Ref. [12].
[b] E_1 from present study was used to calculate Poisson's ratio v_{13} according to Ref. [18].

Values of Poisson's ratio v_{13} in Table 2 vary over a wide range, from −0.171 to 4.958 including even a sign change. Note that the v_{13} values from Refs. [10,12,16–18] were estimated from the compliance components S_{13} and S_{11}. The compliance S_{13} in [10] was directly measured from simple tension tests on pyrolytic graphite specimens, but as discussed with their shear modulus G_{13} results, their specimens contained defects of the mobile dislocations in the basal plane, so that the S_{13} in [10] may not be correct for perfect graphite. The v_{13} values in Refs. [16–18], higher than 0.5 or even 2.0, are theoretically possible, because Poisson's ratio for anisotropic elastic materials may not be bounded [28]. In [18], particularly, the compliance S_{13} was estimated from the thermal expansion coefficients of graphite, accounting for the Poisson's ratio effect on the negative thermal expansion coefficient in the basal plane below 400 °C. However, Kelly [29] expressed doubts about the S_{13} in [18] by showing that the negative thermal expansion is not mainly caused by the Poisson's ratio effect. He made an excellent prediction of the thermal expansion coefficient in the basal plane even by taking the Poisson's ratio equal to zero. Thus, from [29], it may be deduced that Poisson's ratio is nearly zero. Interestingly, in Ref. [12] v_{13} which was calculated by quantum mechanical analysis is negative. As mentioned in [30], however, considering the thermal expansion or specific heat of graphite, or piezoelectric coefficients of carbon fibers, it may be more reasonable for v_{13} to be positive rather than negative.

Although it is still tentative, we consider that our result for v_{13}, obtained by following the mechanical definition of Poisson's ratio based on the molecular mechanical analysis, is reasonable.

3. Micromechanical analysis and parameter sensitivities

The stiffness of epoxy reinforced with a low concentration of graphite platelets can be calculated using a continuum mechanics approach. This has been demonstrated in a three-phase model [31] using Benveniste's implementation [32] of Mori–Tanaka's method [9] for epoxy reinforced by a low concentration of clay nanoplatelets in both intercalated and exfoliated form. In this study, the graphite platelets can be considered as ellipsoidal inclusions randomly distributed and oriented in the epoxy matrix and only two phases need be considered. This is therefore a straightforward application of Mori–Tanaka's method. A brief description of Benveniste's implementation of Mori–Tanaka's method follows.

The effective stiffness tensor $\mathbf{C}^*$ of a composite can be written as [32]

$$\mathbf{C}^* = \mathbf{C}_1 + V_2\{(\mathbf{C}_2 - \mathbf{C}_1)\mathbf{A}\}, \tag{28}$$

where $\mathbf{C}_1$ is the matrix stiffness tensor, $\mathbf{C}_2$ the inclusion stiffness tensor and V_2 the inclusion volume ratio. Benveniste has shown that for Mori–Tanaka's method the concentration tensor $\mathbf{A}$ can be expressed as

$$\mathbf{A} = \mathbf{A}^{(\mathrm{dil})}\left[V_1\mathbf{I} + V_2\left\{\mathbf{A}^{(\mathrm{dil})}\right\}\right]^{-1}, \tag{29}$$

where $V_1 = 1 - V_2$ is the matrix volume ratio and $\mathbf{I}$ the fourth order unity tensor. $\mathbf{A}^{(\mathrm{dil})}$ is the concentration tensor for dilute solution and can be written as

$$\mathbf{A}^{(\mathrm{dil})} = [\mathbf{I} + \mathbf{S}\mathbf{C}_1^{-1}(\mathbf{C}_2 - \mathbf{C}_1)]^{-1}, \tag{30}$$

where **S** is the Eshelby's tensor [33,34]. Curly braces denote average over all possible orientations, or

$$\{\bullet\} = \frac{1}{8\pi^2}\int_0^{2\pi}\int_0^{2\pi}\int_0^{\pi} \bullet f(\theta,\phi,\psi)\sin\theta\,\mathrm{d}\theta\,\mathrm{d}\phi\,\mathrm{d}\psi, \qquad (31)$$

where $f(\theta,\phi,\psi)$ is the orientation distribution function in terms of Euler's angles θ, ϕ and ψ. Since the graphite platelets are assumed to be randomly oriented in the epoxy matrix, the distribution function $f(\theta,\phi,\psi)$ is uniform and given by

$$f(\theta,\phi,\psi) = 1. \qquad (32)$$

This approach has been shown to work reasonably well [31] for stiffness prediction of epoxy reinforced with a low concentration of nanoplatelets as long as reliable information of constituent properties and morphology is available.

As discussed in the preceding section, the elastic parameters of graphite platelets reported in the literature including those of the current study, vary over a wide range. This leads to a natural question about the sensitivity of the nanocomposite modulus to the graphite elastic parameters. Here, we will look into the effect of the five independent elastic parameters (E_1, E_3, G_{13}, ν_{12} and ν_{13}) of graphite platelets on the nanocomposite modulus.

Fig. 7 shows the effects of individually varied platelet elastic parameters on the Young's modulus of epoxy reinforced with 1 wt% graphite nanoplatelets. A lateral dimension to thickness aspect ratio of 200 was used for the graphite platelets having a density of 2.25 g/cm^3. For the epoxy matrix, a Young's modulus of 3.27 GPa, Poisson's ratio of 0.34, and density of 1.17 g/cm^3 were used.

The calculations were conducted by the Mori–Tanaka method described above. The graphite platelet properties used for the reference data are based on the results of the present study, see Tables 1 and 2. At all times, only one graphite elastic parameter was allowed to vary from the set of reference properties. The parameter ranges shown in Fig. 7 correspond to the data variations found in the literature. From Fig. 7, it can be seen that, within the range of reported values of the parameters, the nanocomposite modulus is more sensitive to E_1 and G_{13}, less sensitive to ν_{12} , and completely insensitive to E_3 and ν_{13}.

The difference in sensitivity of the nanocomposite modulus to the various graphite platelet parameters can be understood from the volume averaging process involved in the modulus prediction. The overall deformation of the nanocomposite under loading can be considered as a volume average of individual phase deformations. The higher nanocomposite modulus sensitivity to E_1 and G_{13} (and ν_{12} to a lesser extent for its small range under consideration) is due to the magnification effect of the large lateral platelet dimension on the corresponding deformations, the in-plane extension for E_1 and shear between graphene sheets for G_{13}. On the other hand, the nanocomposite modulus is insensitive to E_3 and ν_{13} because the small platelet thickness minimizes the effect on the corresponding through-thickness deformation.

4. Experimental verification

For the epoxy matrix, the stiffness properties (Young's modulus = 3.27 GPa and Poisson's ratio = 0.34) were

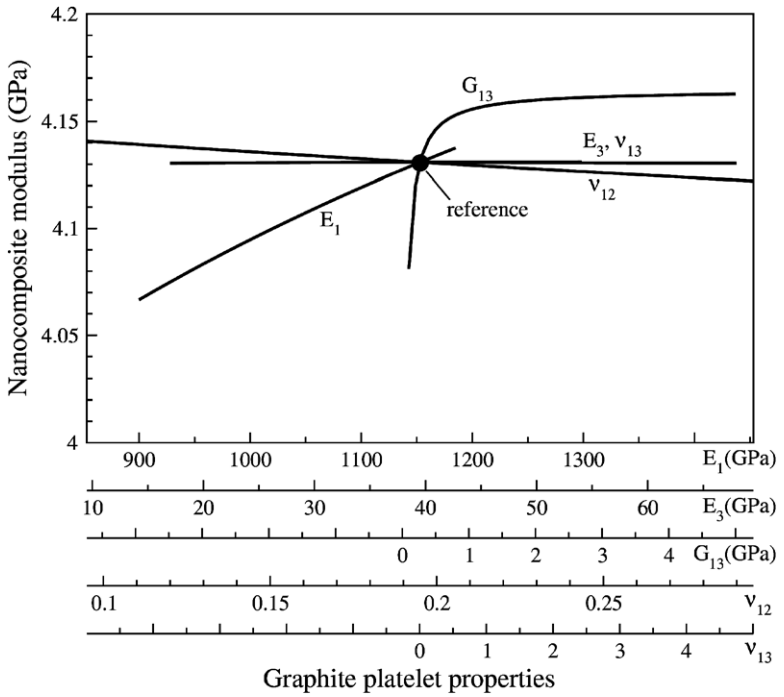

Fig. 7. Effects of individually varied platelet elastic parameters E_1, E_3, G_{13}, ν_{12} and ν_{13} on the Young's modulus of epoxy reinforced with 1 wt% of graphite nanoplatelets with average aspect ratio of 200.

obtained from tensile tests. The stiffness properties of graphite platelets were obtained from molecular mechanical calculations, with results listed in Tables 1 and 2. The graphite platelets were approximated as ellipsoidal inclusions with average lateral size ($a_1 = a_2$) and thickness (a_3) obtained by scanning electronic microscopy. Three different batches of graphite platelet/epoxy composites were prepared, as-received graphite 100GNP/Epoxy, exfoliated graphite 100GNP/Epoxy, and expanded graphite 40GNP/Epoxy. By considering the particles as circular disks, the mean diameter of the as-received and exfoliated 100GNP particles was estimated to be about 1 μm and the aspect ratios were approximated as 5 and 70 for the as-received and exfoliated particles, respectively. The expanded 40GNP graphite particles had a mean diameter of approximately 20 μm and an aspect ratio of roughly 200.

Each batch was ultrasonically mixed with an epoxy system, which consisted of epoxy resin DGEBA (GY6010), anhydride hardener (Aradur 917), and accelerator (DY070) that are typically mixed in the ratio of 100:90:1 by weight, respectively. The mixture was degassed prior to curing. The graphite platelet weight ratio of all batches was 1%, which corresponds to a 0.523% volume ratio. The measured density of the epoxy is 1.17 g/cm^3 and that of the graphite is 2.25 g/cm^3. After curing, dog-bone shaped tensile test specimens were cut from a panel by means of a water-jet and tested in a servo-hydraulic testing machine.

Fig. 8 shows that the elastic moduli obtained experimentally compared very well with the theoretical prediction by the Mori–Tanaka method. As expected from continuum mechanics, it is shown in Fig. 8 that the moduli of nanocomposites with randomly oriented ellipsoidal inclusions depend on the aspect ratio (lateral size divided by thickness), and not on the size of the inclusion. It is understood that the validity of the Mori–Tanaka approach is limited to dilute concentrations of non-interacting particles. For a nanocomposite containing uniformly dispersed and randomly oriented platelets, the continuum approach above is valid up to a critical particle volume fraction which is inversely proportional to the particle aspect ratio. In other words, for a given particle concentration the predictions are valid up to a certain particle aspect ratio. For the case illustrated in Fig. 8, the limiting aspect ratio would be on the order of 300.

5. Conclusion

A set of elastic constants of graphite nanoplatelets was calculated based on their molecular force field. They were in good agreement with both experimental data and other published theoretical predictions, except for the out-of-plane shear modulus G_{13} and Poisson's ratio v_{13}. It was confirmed that using the Lennard–Jones potential underestimates the shear modulus G_{13} for perfect graphite. Poisson's ratio v_{13} obtained in this study is positive and very small (0.006) and falls within the wide range of the literature data.

Moduli of epoxy reinforced with graphite nanoplatelets were predicted by the Mori–Tanaka method using the graphite elastic properties obtained by molecular mechanics. The predictions are in very good agreement with experimental results for various reinforcing graphite particle sizes and aspect ratios. It was confirmed that the nanocomposite moduli depend strongly on the aspect ratio of the reinforcing particles.

It was found that the nanocomposite modulus is completely insensitive to the variation of out-of-plane modulus E_3 and Poisson's ratio v_{13} of the nanoplatelet, both related to out-of-plane through-thickness deformations. The nanocomposite modulus is more sensitive to the in-plane

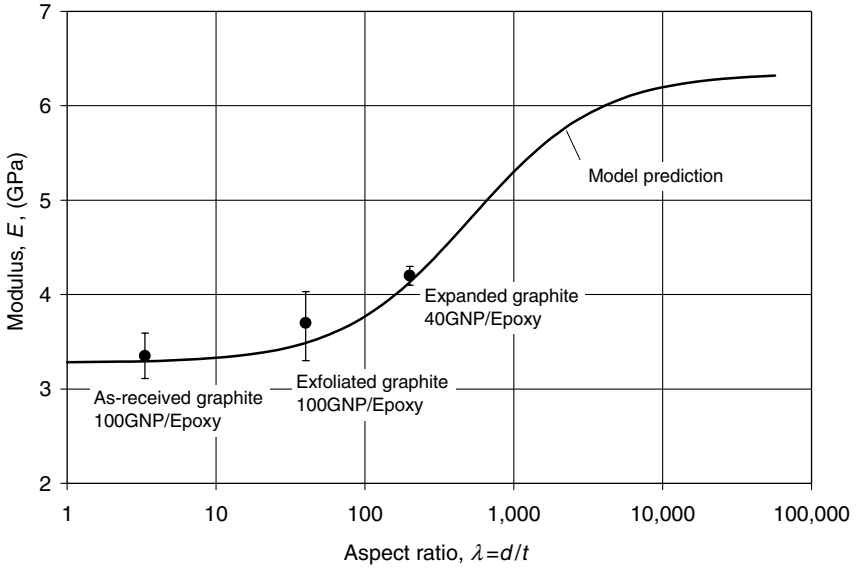

Fig. 8. Predicted and measured Young's modulus of epoxy reinforced with various graphite nanoplatelets for a particle concentration of 1 wt%.

modulus E_1 and out-of-plane shear modulus G_{13} (and v_{12} to a lesser extent for its small range under consideration) due to the magnification effect of the large lateral platelet dimension on the corresponding deformation.

Acknowledgement

We gratefully acknowledge the grant support from the NASA University Research, Engineering and Technology Institute on Bio Inspired Materials (BIMat) under award No. NCC-1-02037.

References

[1] Yasmin A, Luo JJ, Daniel IM. Processing of expanded graphite reinforced polymer nanocomposites. Compos Sci Technol 2006;66(9):1182–9.
[2] Odegard GM, Gates TS. Modeling and testing of the viscoelastic properties of a graphite nanoplatelet/epoxy composite. J Intell Mater Syst Struct 2006;17(3):239–46.
[3] Li J, Kim JK, Sham ML. Conductive graphite nanoplatelet/epoxy nanocomposites: effects of exfoliation and UV/ozone treatment of graphite. Scripta Mater 2005;53(2):235–40.
[4] Hung MT et al. Heat conduction in graphite-nanoplatelet-reinforced polymer nanocomposites. Appl Phys Lett 2006;89(2):023117.
[5] Odegard GM, Clancy TC, Gates TS. Modeling of the mechanical properties of nanoparticle/polymer composites. Polymer 2005;46(2):553–62.
[6] Sheng N et al. Multiscale micromechanical modeling of polymer/clay nanocomposites and the effective clay particle. Polymer 2004;45(2):487–506.
[7] Gao XL, Li K. A shear-lag model for carbon nanotube-reinforced polymer composites. Int J Solids Struct 2005;42(5–6):1649–67.
[8] Li CY, Chou TW. Multiscale modeling of carbon nanotube reinforced polymer composites. J Nanosci Nanotechnol 2003;3(5):423–30.
[9] Mori T, Tanaka K. Average stress in matrix and average elastic energy of materials with misfitting inclusions. Acta Metall 1973;21(5):571–4.
[10] Blakslee OL, Proctor DG, Seldin EJ, Spence GB, Weng T. Elastic constants of compression-annealed pyrolytic graphite. J Appl Phys 1970;41(8):3373–82.
[11] Dolling G, Brockhouse BN. Lattice vibrations in pyrolitic graphite. Phys Rev B 1962;128(3):1120–3.
[12] Jansen HJF, Freeman AJ. Structural and electronic properties of graphite via an all-electron total-energy local-density approach. Phys Rev B 1987;35(15):8207–14.
[13] Jenkins GM, Jouquet G. The effect of short-term neutron irradiation on the shear compliance of hot-worked pyrolytic graphite. Carbon 1968;6:85–8.
[14] Kelly BT, Duff MJ. On the validity of Lennard–Jones potentials for the calculation of elastic properties of a graphite crystal. Carbon 1970;8:77–83.
[15] Komatsu K. Interpretation of the specific heat of various graphites at very low temperature. J Phys Chem Solids 1964;25:707–12.
[16] Spence GB. In: Proceedings of the fifth conference on carbon, 1961.
[17] Zhao YX, Spain IL. X-ray diffraction data for graphite to 20 GPa. Phys Rev B 1989;40(2):993–7.
[18] Riley DP. The thermal expansion of graphite: part II. Theoretical. Proc Phys Soc 1945;57:486–95.
[19] Lévy F. Intercalated layered materials. Phys Chem Mater Layered Struct 1979;6:323–421.
[20] Chung DDL. Review graphite. J Mater Sci 2002;37:1475–89.
[21] Chang T, Gao H. Size-dependent elastic properties of a single-walled carbon nanotube via a molecular mechanics model. J Mech Phys Solids 2003;51:1059–74.
[22] Brenner DW. Empirical potential for hydrocarbons for use in simulating the chemical vapor-deposition of diamond films. Phys Rev B 1990;42:9458–71.
[23] Yao Z et al. Mechanical properties of carbon nanotube by molecular dynamics simulation. Comput Mater Sci 2001;22:180–4.
[24] Belytschko T et al. Atomistic simulations of nanotube fracture. Phys Rev B 2002;65:235–43.
[25] Xiao JR, Gama BA, Gillespie Jr JW. An analytical molecular structural mechanics model for the mechanical properties of carbon nanotubes. Int J Solids Struct 2005;42:3075–92.
[26] Girifalco LA, Lad RA. Energy of cohesion, compressability, and the potential energy functions of the graphite system. The J Chem Phys 1956;25(4):693–7.
[27] Agranovich VM, Semenov LP. A contribution of the theory of the effect of irradiation on certain properties of graphite. J Nucl Energy Parts A/B 1964;18:141–7.
[28] Ting TCT, Chen TY. Poisson's ratio for anisotropic elastic materials can have no bounds. Quart J Mech Appl Math 2005;58:73–82.
[29] Kelly BT. The thermal expansion coefficient of graphite parallel to the basal planes. Carbon 1972;10:429–33.
[30] Goldberg HA. Final Report to US Army Research Office, 1985.
[31] Luo JJ, Daniel IM. Characterization and modeling of mechanical behavior of polymer/clay nanocomposites. Compos Sci Technol 2003;63(11):1607–16.
[32] Benveniste Y. A New approach to the application of Mori–Tanaka theory in composite-materials. Mechan Mater 1987;6(2):147–57.
[33] Eshelby JD. The determination of the elastic field of an ellipsoidal inclusion, and related problems. Proc Roy Soc London Ser A—Math Phys Sci 1957;241(1226):376–96.
[34] Mura T. Micromechanics of defects in solids. 2nd ed. Boston: Nijhoff; 1987.